A Real-Time Measuring Method of Translational/Rotational Velocities of a Flying Ball

Akira Nakashima * **Yoji Tuda** * **Chunfang Liu** *
Yoshikazu Hayakawa *,**

* *Mechanical Science and Engineering, Graduate School of
Engineering, Nagoya University, Furo-cho, Chikusa-ku, Nagoya, Japan
(e-mail: a_nakashima@nuem.nagoya-u.ac.jp)*
** *RIKEN-TRI Collaboration Center, RIKEN, 2271-103, Anagahora,
Shimoshidami, Moriyama-ku, Nagoya, Japan.*

Abstract: We propose a real-time measuring method of both the translational/rotational velocities of a flying ball using two high speed cameras. The rotational velocity is estimated by the kinematics which relates the velocity to the position variation of the centroid of a feature area marked on the ball. The position variation is calculated by the correlation between two images with respect to the translational displacement in the images. The corresponding 3D position of the feature area is necessary for the estimation by the kinematics. It is calculated by the centroids of all the feature areas on the ball in the left and right images with the assumption where the centroids coincide with each other in the 3D space. The proposed method is verified with respect to some configurations of the cameras and texture patterns of the feature areas by numerical simulations. The effectiveness of the method is verified by experiments.

Keywords: speed measurement, computer vision, real-time, image matching

1. INTRODUCTION

It is a challenging task for a robot to play table tennis with a human because playing table tennis is a dexterous task for humans. For simplicity, consider the situation of Fig. 1, where a robot tries to hit a flying ball. The strategy of the robot playing table tennis can be decomposed as the following subtasks: 1) To detect the states of the flying ball with vision sensors; 2) To predict the ball trajectory; 3) To determine the trajectory of the racket attached to the robot for hitting the ball to achieve desired ball trajectory. The number 1) means the image processing algorithm to obtain the position, the translational and rotational velocities of the ball. The number 2) means the prediction of the position and translational/rotational velocities of the ball at the time for the robot to hit the ball. The number 3) means the determination of the trajectories of the position and orientation of the racket for the ball to follow desired trajectory. The algorithm in the subtask 1) is necessary to be performed *in real time* for the next task. In the subtasks

Fig. 1. A robot tries to hit a flying ball.

2) and 3), the ball *rebounds* from the table and the racket rubber. It is therefore necessary to model the rebound phenomena between the ball and the table/rubber in order to achieve the subtasks 2) and 3). The rebound models have been proposed by Nakashima et al. (2009, 2010). This paper is concerned with the real-time measurement of the rotational/translational velocities of the ball.

A vision sensor is effective with the measurement of the velocities of the ball since it is a non-contact sensor and can measure both the translational/rotational velocities while an optical rotation meter can not measure both them at the same time. It is necessary that some textures are marked on the ball as feature areas in order to detect the movement of the ball by the vision sensors. It is also necessary that the sampling frequency of a vision sensor is high since the rotational velocity of the ball is very large, e.g., 2000–3000 [rpm] in the case of amateur players or 3000–5000 [rpm] in the case of pro players (Tamaki et al. (2004)). Nakabo et al. (1996) developed a high speed vision camera with the sampling frequency 1000 [Hz] and the resolution 128×128 [pixel] and applied it to high speed target tracking. Watanabe et al. (2005) proposed a *real-time* measuring method of the rotational velocity with the high speed camera in the case where the position of the ball is fixed. They achieved measuring the velocity under 1200 [rpm]. In their method, the kinematics is used which relates the rotational velocity to the position variation of the centroid of the feature area. The position variation is calculated by tracking the feature area in two images with the self-windowing of Ishii et al. (1996), where it is assumed that a feature area in

one image laps over the corresponding area in the other image of the next frame. This technique is called as the *tracking-based method* in this paper. It is also necessary to calculate the corresponding 3D position of the feature area in order to use the kinematics. They obtained it by assuming that the optic axis is through the center of the ball. On the other hand, Tamaki et al. (2004) measured the rotational velocity by an *off-line* processing with the *image registration* (Szeliski (1994)) and the knowledge of the ball shape. The image registration estimates the homogeneous transformation matrix of a point on the ball form an image to the other by minimizing the sum of the squares of the intensity residuals between the two images with a nonlinear optimization. The rotational velocity is calculated by the estimated rotation matrix.

In the tracking-based method, it is necessary to track a feature area in two images in order to calculate the corresponding position variation. However, the self-windowing used by Watanabe et al. (2005) can not be applied because the feature area in the two images does not lap over each other in the case where the spin of the ball is larger than 2000 [rpm]. Furthermore, the translational velocity can not be measured because of the assumption of the fixed center of the ball. The image registration can measure the velocity 5000 [rpm] as in the results of Tamaki et al. (2004) since it does not require tracking a feature area in two images. However, it is difficult to apply it in real-time because of the nonlinear optimization for obtaining the homogeneous transformation.

Therefore, we propose a real-time measuring method of both the translational/rotational velocities of the ball using the two high speed cameras without tracking. The rotational velocity is estimated by the kinematics and a representative position variation of all the feature areas, which is calculated by the correlation between the two images with respect to the translational displacement in the images. The cost of the calculation is small because the calculation does not estimate the homogeneous transformation. The corresponding 3D position of the feature area is estimated by the centroids of all the feature areas on the ball in the left and right images with the assumption where the centroids coincide with each other in the 3D space.

The target system and preliminary are shown in Section 2. The tracking-based method is briefly described in Section 3. The real-time measuring method is proposed in Section 4. In Section 5, the proposed method is verified with respect to some configurations of the cameras by numerical simulations. An appropriate configuration for the method is determined. Appropriate texture patterns of the feature areas are also verified here. In Section 6, the method is verified by experiments. It is checked whether the processing time is shorter than usual rally time or not. Conclusions are shown in Section 7.

2. SYSTEM CONFIGURATION AND PRELIMINARY

2.1 System Configuration

Figure 2 shows the experimental system and the coordinate frames. The table is an international standard one with the size of $1525(\text{W}) \times 760(\text{H}) \times 2740(\text{D})$ [mm]. The
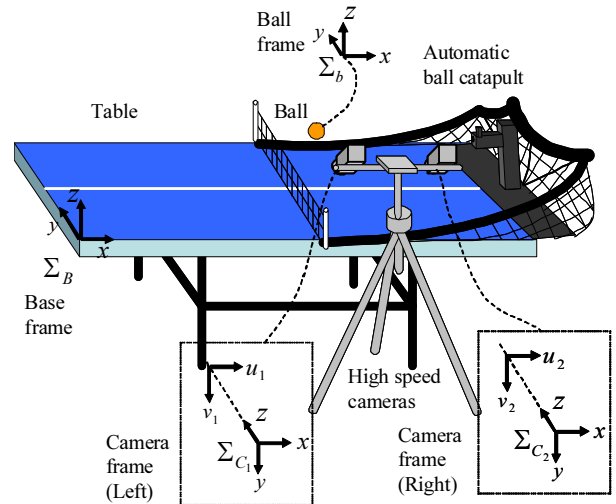
Fig. 2. The experimental system and the frame configurations.
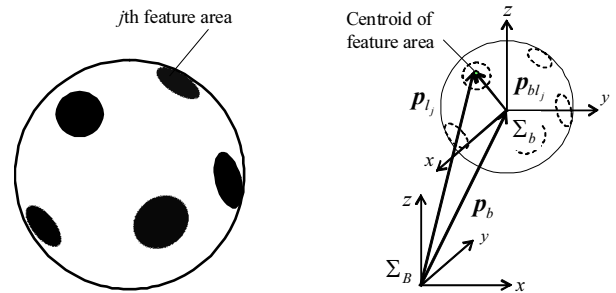
Fig. 3. The feature areas on the ball and the position of the centroid.

parameters of a ping-pong ball are $m = 2.7 \times 10^{-3}$[kg] and $r = 2.0 \times 10^{-2}$[m]. The ball is shot out from the automatic ball catapult of ROBO-PONG 2040 (SAN-EI Co.) which is set at the end of the table. The flying ball is measured by the two high-speed cameras with 980 [fps] (Hamamatsu Photonics K.K.). The array and pixel sizes per meter are 232×232 and $\alpha_u, \alpha_v = 2.0 \times 10^{-5}$ [pixel/m]. The focal length of the lens is $f = 3.5 \times 10^{-2}$ [m]. The sampled data are quantized as 2D image coordinates with the monochrome brightness of 8bit (0–255). Σ_B is the reference frame at the corner of the table. Σ_{C_i} $(i = 1, 2)$ are the camera frames with their z-axes coinciding with the optical axes. $\boldsymbol{\xi}_i := [u_i \ v_i]^{\mathrm{T}} \in \mathbb{R}^2$ is the image coordinates of the ith camera. The frames Σ_{C_i} are calibrated with respect to Σ_B. Figure 3 shows feature areas on the ball $(j = 1, \cdots, N_l)$. Σ_b is the frame attached to the center of the ball. $\boldsymbol{p}_b \in \mathbb{R}^3$ is the position of the center of the ball with respect to Σ_B. The feature position $\boldsymbol{p}_{l_j} \in \mathbb{R}^3$ is the centroid of the jth feature area with respect to Σ_B $(j = 1, \cdots, M)$. The corresponding image coordinate of $\boldsymbol{p}_{l_j}$ is defined as $\boldsymbol{\xi}_{l_j} \in \mathbb{R}^2$. The relative feature position is defined as $\boldsymbol{p}_{bl_j} := \boldsymbol{p}_{l_j} - \boldsymbol{p}_b$.

In latter, we assume that there is no effect of the air resistance. Therefore, the translational/rotational velocities of the ball are invariant during measuring the flying ball by the cameras.

(a)   (b)

(c)   (d)
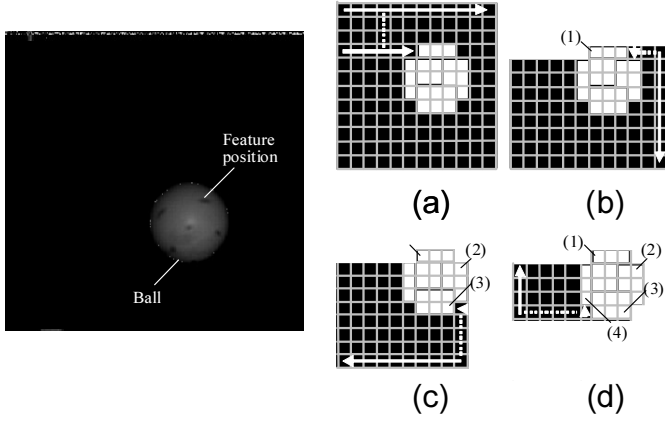
Fig. 4. Image data and Detection of the center of the ball.

2.2 Basic Relations

A 3D position $^{C_i}\boldsymbol{p} \in \mathbb{R}^3$ expressed in Σ_{C_i} is projected to the corresponding image coordinate $\boldsymbol{\xi}_i \in \mathbb{R}^2$ as

$$\boldsymbol{\xi}_i = \begin{bmatrix} u_i \\ v_i \end{bmatrix} = \frac{f}{p_{z_i}} \begin{bmatrix} \frac{p_{x_i}}{\alpha_u} \\ \frac{p_{y_i}}{\alpha_v} \end{bmatrix}, \qquad (1)$$

where $^{C_i}\boldsymbol{p} := [p_{x_i} \ p_{y_i} \ p_{z_i}]^{\mathrm{T}}$. $^{C_i}\boldsymbol{p}$ is related to $^B\boldsymbol{p} \in \mathbb{R}^3$ expressed in Σ_B by the homogeneous transformation:

$$^{C_i}\boldsymbol{p} = {}^{C_i}\boldsymbol{p}_B + \boldsymbol{R}_{C_i B}{}^B\boldsymbol{p}, \qquad (2)$$

where $^{C_i}\boldsymbol{p}_B \in \mathbb{R}^3$ and $\boldsymbol{R}_{C_i B}$ are the position and rotation matrix of Σ_B with respect to Σ_{C_i}. The pair of $\left(^{C_i}\boldsymbol{p}_B, \boldsymbol{R}_{C_i B}\right)$ is obtained by the calibration of Σ_{C_i} with respect to Σ_B.

3. TRACKING-BASED METHOD

The tracking-based measuring method is briefly described here. The image processing and variables are described with respect to only one of the images of the two cameras because they are the same as the other one. Then, the subscript i is dropped. The calculation of $\boldsymbol{\xi}_{l_j}$ from the jth feature area is omitted for space limitation. It is assumed that any feature points are tracked in every frame.

3.1 Estimation of the translational velocity

The left of Fig. 4 shows an example of the image data of the camera. Let us consider the detection of the center of the ball. Since the ball is white and the background is much darker than the ball, all the area of the ball can be easily detected by the simple scanning shown in the right of Fig. 4. In the scanning of (a), the arrays of the image are scanned in turn from the left and top until the brightness of the scanned image is larger than a specified threshold for detecting the while area of the ball. The scanning of (b)–(d) are similar to the one of (a). The positions of the detected data as the parts of the white area with the threshold are recorded as $\boldsymbol{\xi}_i := (u_i, v_i) \in \mathbb{R}^2 \ (i = 1, \cdots, 4)$. Consider the mediators of the lines between $\boldsymbol{\xi}_{i+1}$ and $\boldsymbol{\xi}_i$ $(i = 1, \cdots, 4)$, $\boldsymbol{\xi}_5 := \boldsymbol{\xi}_1$ as shown in the left of Fig. 5. Define $\boldsymbol{\xi}_c$ as the center of the ball. The center $\boldsymbol{\xi}_c$ is estimated by the least squares method with the following performance function:
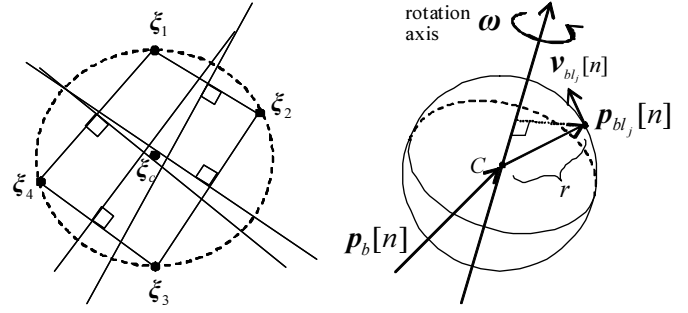
Fig. 5. Detection of the translation and rotation velocities.

$$V_c(\boldsymbol{\xi}_c) := \sum_{i=1}^4 \frac{\left| (\boldsymbol{\xi}_{i+1} - \boldsymbol{\xi}_i)^{\mathrm{T}} \boldsymbol{\xi}_c - \frac{1}{2}(\|\boldsymbol{\xi}_{i+1}\|^2 - \|\boldsymbol{\xi}_i\|^2) \right|^2}{\|\boldsymbol{\xi}_{i+1} - \boldsymbol{\xi}_i\|^2},$$
$$(3)$$

which is the sum of the squares of the distances of $\boldsymbol{\xi}_c$ from the mediators. The center of the ball $\boldsymbol{p}_b$ is calculated by $\boldsymbol{\xi}_c$ in the left and right images. The translational velocity of the ball is obtained by the mean of all the velocities between the $(n + 1)$th and nth position as

$$\boldsymbol{v}_b = \frac{\sum_{i=2}^N \boldsymbol{v}_b[n]}{N - 1}, \ \boldsymbol{v}_b[n] := \frac{\boldsymbol{p}_b[n] - \boldsymbol{p}_b[n-1]}{\Delta t}, \quad (4)$$

where $\Delta t = 1/980$ [s] is the sampling time and N is the number of the frames used for the data processing. Note that $[n]$ denotes the nth frame.

3.2 Estimation of the rotational velocity

Next, consider the calculation of the rotational velocity of the ball. The right of Fig. 5 shows the ball in the nth frame, where $\boldsymbol{\omega} \in \mathbb{R}^3$ is the rotation axis. For the jth feature point, the following rotational relationship is hold by Murray et al. (1994):

$$\boldsymbol{p}_{bl_j}[n] = e^{\widehat{\boldsymbol{\omega}}\Delta t}\boldsymbol{p}_{bl_j}[n-1], \ e^{\widehat{\boldsymbol{\omega}}\Delta t} \approx \boldsymbol{I}_3 + \widehat{\boldsymbol{\omega}}\Delta t, \quad (5)$$

where $\widehat{\boldsymbol{\omega}} \in \mathbb{R}^{3\times 3}$ is the skew-symmetric matrix which corresponds to the cross product of $\boldsymbol{\omega}$. Note that $e^{\widehat{\boldsymbol{\omega}}\Delta t}$ is linearized due to the small Δt. (5) is rewritten as

$$\widehat{\boldsymbol{p}}_{bl_j}[n]\boldsymbol{\omega} = -\boldsymbol{v}_{bl_j}[n], \ \boldsymbol{v}_{bl_j}[n] := \frac{\boldsymbol{p}_{bl_j}[n] - \boldsymbol{p}_{bl_j}[n-1]}{\Delta t}. \quad (6)$$

The rotational velocity $\boldsymbol{\omega}$ is obtained by solving the linear least squares method with the performance function which is the sum of the square of the difference between both the terms of (6). The analytical solution of the linear least ssquares method is given by

$$\boldsymbol{\omega} = (\boldsymbol{A}^{\mathrm{T}}\boldsymbol{A})^{-1}\boldsymbol{A}^{\mathrm{T}}\boldsymbol{b}, \qquad (7)$$

where

$$\boldsymbol{A} := \begin{bmatrix} \widehat{\boldsymbol{p}}_{bl_1}[2] \\ \vdots \\ \widehat{\boldsymbol{p}}_{bl_1}[N] \\ \vdots \\ \widehat{\boldsymbol{p}}_{bl_M}[2] \\ \vdots \\ \widehat{\boldsymbol{p}}_{bl_M}[N] \end{bmatrix}, \ \boldsymbol{b} := \begin{bmatrix} -\boldsymbol{v}_{bl_1}[2] \\ \vdots \\ -\boldsymbol{v}_{bl_1}[N] \\ \vdots \\ -\boldsymbol{v}_{bl_M}[2] \\ \vdots \\ -\boldsymbol{v}_{bl_M}[N] \end{bmatrix}.$$

4. REAL-TIME MEASURING METHOD

The estimation of the translational velocity is same as the one in Section 3. The estimation of the rotational velocity with the correlation between the images in the two frames is proposed here.

4.1 Kinematics between the image coordinates and the rotational velocity

Substituting (2) into (1) yields

$$u_i = \frac{f}{\alpha_u} \frac{r_{11}{}^B p_{x_i} + r_{12}{}^B p_{y_i} + r_{13}{}^B p_{z_i} + {}^{C_i} p_{Bx_i}}{r_{31}{}^B p_{x_i} + r_{32}{}^B p_{y_i} + r_{33}{}^B p_{z_i} + {}^{C_i} p_{Bz_i}},$$

$$v_i = \frac{f}{\alpha_u} \frac{r_{21}{}^B p_{x_i} + r_{22}{}^B p_{y_i} + r_{23}{}^B p_{z_i} + {}^{C_i} p_{Bx_i}}{r_{31}{}^B p_{x_i} + r_{32}{}^B p_{y_i} + r_{33}{}^B p_{z_i} + {}^{C_i} p_{Bz_i}}, \quad (8)$$

where r_{ij} is the component of $\boldsymbol{R}_{C_i B}$. Differentiating (8) of $i = 1, 2$ and combining the resultant equations lead to

$$\dot{\boldsymbol{\xi}} = \boldsymbol{J}({}^B \boldsymbol{p}){}^B \dot{\boldsymbol{p}}, \quad (9)$$

where $\boldsymbol{\xi} := [\boldsymbol{\xi}_1^{\mathrm{T}} \ \boldsymbol{\xi}_2^{\mathrm{T}}]^{\mathrm{T}} \in \mathbb{R}^4$ and $\boldsymbol{J} \in \mathbb{R}^{4 \times 3}$ is the image jacobian. Replacing $(\boldsymbol{\xi}, {}^B \boldsymbol{p})$ to the feature point $(\boldsymbol{\xi}_{l_j}, \boldsymbol{p}_{l_j})$ leads to

$$\dot{\boldsymbol{\xi}}_{bl_j} + \dot{\boldsymbol{\xi}}_c = \boldsymbol{J}(\boldsymbol{p}_{l_j})(\dot{\boldsymbol{p}}_{bl_j} + \dot{\boldsymbol{p}}_b), \quad (10)$$

where $\boldsymbol{\xi}_{bl_j} := \boldsymbol{\xi}_{l_j} - \boldsymbol{\xi}_c$ is the relative feature position vector in the 2D image planes which corresonds to $\boldsymbol{p}_{bl_j}$. Note therefore that these 2D and 3D feature potition variables $\boldsymbol{\xi}_c$ and $\boldsymbol{p}_b$ are related by

$$\dot{\boldsymbol{\xi}}_c = \boldsymbol{J}(\boldsymbol{p}_{l_j})\dot{\boldsymbol{p}}_b. \quad (11)$$

Substituting (11) into (10) and transforming the resultant equation to the discrete formulation result in

$$\Delta \boldsymbol{\xi}_{bl_j}[n] = \boldsymbol{J}(\boldsymbol{p}_{l_j}[n])\Delta \boldsymbol{p}_{bl_j}[n], \quad (12)$$

where

$$\Delta \boldsymbol{\xi}_{bl_j}[n] := \boldsymbol{\xi}_{bl_j}[n] - \boldsymbol{\xi}_{bl_j}[n-1]$$
$$\Delta \boldsymbol{p}_{bl_j}[n] := \boldsymbol{p}_{bl_j}[n] - \boldsymbol{p}_{bl_j}[n-1].$$

Substituting (6) into (12) results in

$$\Delta \boldsymbol{\xi}_{bl_j}[n] = -\boldsymbol{J}(\boldsymbol{p}_{l_j}[n])\widehat{\boldsymbol{p}}_{bl_j}[n]\boldsymbol{\omega}\Delta t. \quad (13)$$

Solving (13) with respect to $\boldsymbol{\omega}$, we get the following kinematic relationship

$$\boldsymbol{\omega} = -\left(\boldsymbol{J}(\boldsymbol{p}_{l_j}[n])\widehat{\boldsymbol{p}}_{bl_j}[n]\right)^{+} \frac{\Delta \boldsymbol{\xi}_{bl_j}[n]}{\Delta t}. \quad (14)$$

A matrix $\boldsymbol{A}^{+}$ stands for the pseudo inverse matrix of $\boldsymbol{A}$. Note that $\boldsymbol{p}_{l_j}[n]$ can be calculated by $\boldsymbol{p}_{bl_j}[n]$ and $\boldsymbol{p}_b[n]$ with $\boldsymbol{p}_{l_j}[n] = \boldsymbol{p}_{bl_j}[n] + \boldsymbol{p}_b[n]$. However, as mentioned in Section 1, $\boldsymbol{p}_{bl_j}[n]$ and $\boldsymbol{\xi}_{bl_j}[n]$ can not be obtained and $\boldsymbol{\xi}_{bl_j}[n]$ can not be corresponded to the previous one because it is impossible to track the feature areas. In the following, the estimation methods of $\Delta \boldsymbol{\xi}_{l_j}[n]$ and $\boldsymbol{p}_{l_j}[n]$.

4.2 Estimation of the image displacement

Define $G_i[n](s,t) \in \mathbb{N}^{232 \times 232}$ as the 2D image data of the nth image of the ith camera. Also define $g_i[n](s,t) \in \mathbb{N}^{N_{g_i} \times N_{g_i}}$ as the segmented 2D image data of the inscribed quadrangle of the ball as shown in Fig. 6. The values of $G_i[n]$ and $g_i[n]$ are assumed to be binarized to $(0,1)$ with an appropriate threshold. The correlation between the nth
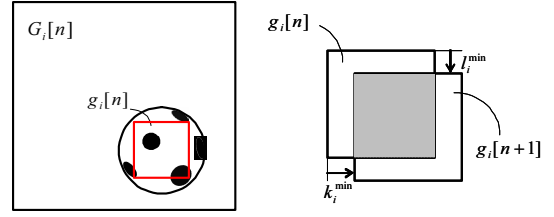

Fig. 6. The segmented 2D image data and the correlation between the two images.

and $(n+1)$th images is given by minimizing the following performance function:

$$V_i(k_i, l_i) := \frac{1}{(N_{g_i} - k_i)(N_{g_i} - l_i)} \times$$
$$\sum_{s=1}^{N_{g_i} - k_i} \sum_{t=1}^{N_{g_i} - l_i} \left(g_i[n+1](s,t) - g_i[n](s+l_i, t+k_i) \right)^2 \quad (15)$$

This operation is illustrated in the right of Fig. 6, where (k_i^{min}, l_i^{min}) is the solution of the correlation. Then, we estimate the image displacements $\Delta \boldsymbol{\xi}_{bl_j}$ of all the feature points by (k_i^{min}, l_i^{min}) of the correlation as

$$\Delta \boldsymbol{\xi}_{bl}[n] = \left[\ k_1^{min}[n] \ \ l_1^{min}[n] \ \ k_2^{min}[n] \ \ l_2^{min}[n] \ \right]^{\mathrm{T}}. \quad (16)$$

The searching ranges of (k_i, l_i) are $K_{min} \leq k_i \leq K_{max}$ and $L_{min} \leq l_i \leq L_{max}$, which are modified in each frame for reducing the processing time. In the first and second frames, the search ranges are set to $K_{min} = L_{min} = -N_g$ and $K_{max} = L_{max} = N_g$. From the third frame, it is assumed that the next (k_i^{min}, l_i^{min}) exists nearby the previous ones. Therefore, the ranges are set to

$$K_{min}[n] = k_i^{min}[n-1] - K', K_{max}[n] = k_i^{min}[n-1] + K' \quad (17)$$

$$L_{min}[n] = l_i^{min}[n-1] - L', \ L_{max}[n] = l_i^{min}[n-1] + L', \quad (18)$$

where K' and L' are chosen as small ones.

4.3 Representative position corresponding to the estimated image displacement

In the previous subsection, we estimated the image displacement by the representative displacement $\Delta \boldsymbol{\xi}_{bl}$ of the image correlation. It is necessary to determine the representative 3D position corresponding to $\Delta \boldsymbol{\xi}_{bl}$ in order to use the kinematics (14) with $\Delta \boldsymbol{\xi}_{bl}$.

Firstly, as in Fig. 7, the centroids of the feature areas are calculated by

$$\boldsymbol{\xi}_{bf_i} = \frac{\sum_{s,t \in \mathcal{D}} G(s,t)[s \ t]^{\mathrm{T}}}{\sum_{s,t \in \mathcal{D}} G(s,t)} - \boldsymbol{\xi}_{c_i}, \quad (19)$$

where

$$\mathcal{D} := \left\{ (s,t) \ \middle| \ \left[\xi_{c_i} - \frac{N_{g_i}}{2} \right] \leq s, t \leq \left[\xi_{c_i} + \frac{N_{g_i}}{2} \right] \right\}$$

and $[\cdot]$ stands for the integer as an argument rounded off. Secondly, the representative 3D position $\boldsymbol{p}_{bl} \in \mathbb{R}^3$ is calculated by the centroids $\boldsymbol{\xi}_{bf_1}$ and $\boldsymbol{\xi}_{bf_2}$. However, this is not a position on the ball because the image centroids do not coincide with each other in the 3D space. This causes the reduction of the accuracy of the rotational velocity by using (14). Therefore, thirdly, $\boldsymbol{p}_{bl}$ is modified to a position
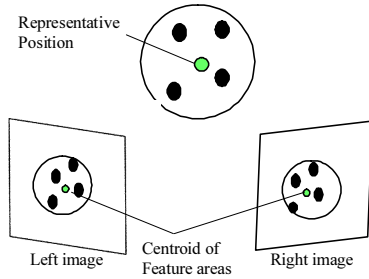
Fig. 7. The representative position of the feature areas.
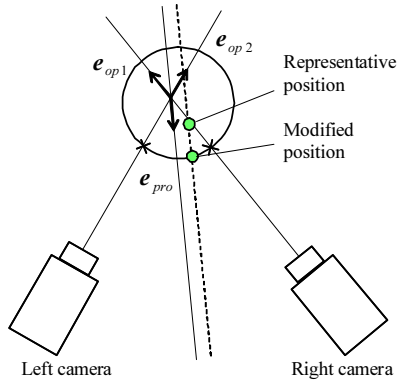
Fig. 8. The modification of the representative position.

on the ball as in Fig. 8. The direction of the projection of $\boldsymbol{p}_{bl}$ on the ball is defined as

$$\boldsymbol{e}_{pro} := -\frac{1}{\sqrt{2}}(\boldsymbol{e}_{op_1} + \boldsymbol{e}_{op_2}), \tag{20}$$

where

$$e_{op_i} := \boldsymbol{R}_{BC_i}[0\ 0\ 1]^{\mathrm{T}},\ i = 1, 2$$

are the normalized vectors in the optical axes of the cameras. Then, the modified position $\boldsymbol{p}'_{bl}$ is given by

$$\boldsymbol{p}'_{bl} = \boldsymbol{p}_{bl} + k\boldsymbol{e}_{pro}, \tag{21}$$

where the value of k is obtained by solving the following constraint:

$$\|\boldsymbol{p}'_{bl}\| = r. \tag{22}$$

r is the radius of the ball.

5. SIMULATION

The proposed method is simulated here. The measurement accuracy of the method is examined under different camera configurations. The parameters of the camera configuration are the distance between cameras d, the angle of the optical axes of the cameras θ and the elevation angle of the cameras α as shown in Fig. 9. The parameters are set to $d = 0.30$ [m], $\theta = 16$ [deg] in order not to increase the
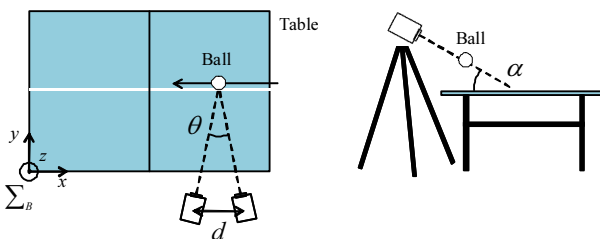
Fig. 9. The camera configuration.

difference between the centroids of the feature areas on the ball in both the images in the 3D space. The value of α is changed from 0 to 90 [deg] with the increment of 30 [deg]. The translational speed is changed from 5 [m/s] to 15 [m/s] with the increment of 5 [m/s]. The translational direction is set to $[-1\ 0\ 0]^{\mathrm{T}}$. The rotational speed is changed from 1500 to 4500 [rpm] with the increment of 1500 [rpm]. The axis of the rotation is the top spin, i.e., $[0\ -1\ 0]^{\mathrm{T}}$.

The results are shown in Figs. 10–12. Fig.10 displays the measured and real values of the translational speed in the x-axis with all the elevation angles. The results in the y and z-axes are omitted because of its trivia. The solid line represents the points that measured and real values coincide with each other. It can be confirmed from Fig.10 that the accuracy of the measured value of translational speed is high regardless of the elevation angles of the
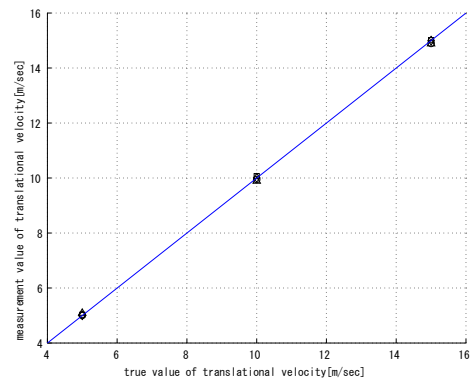
Fig. 10. The translational velocity in the x-axis.
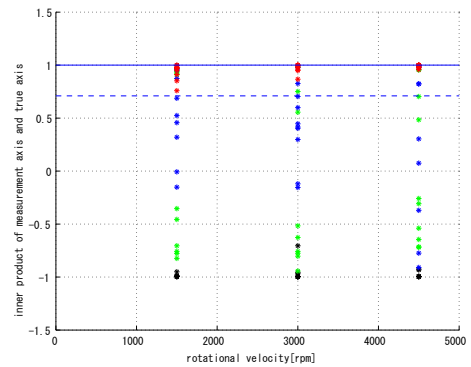
Fig. 11. The inner products between the true and measured rotational axes.
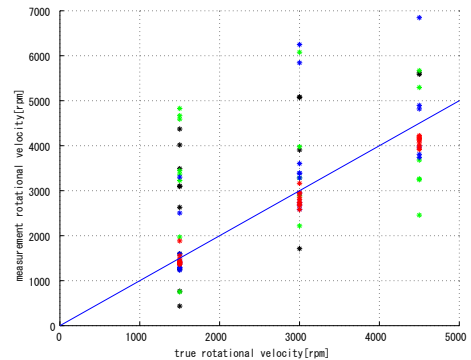

Fig. 12. The rotational speed.

camera. Figs. 11, 12 show the inner product between the measured and true value of the rotational axis and measurements of the rotational speed respectively. The black, green, blue and red markers represent 0, 30, 60 and 90 [deg] of the elevation angles. In Fig. 11, the solid line and dashed line represent the points that values of inner product are 1 and $1/\sqrt{2}$ respectively. The measured values on the solid line coincide the true values. The solid line in Fig. 12 represents the points that measured and real values coincide with each other. In the case of the angle of $\alpha = 90$ [deg], the accuracy of the measurement is best; the angle between the measured and true the rotation axes is smaller than 45 [deg] and the difference between the measured and true speeds is smaller than 600 [rpm]. This is because the optical axes are perpendicular to the rotation axis. However, the angel $\alpha = 90$ [deg] is not appropriate because the ranges of the images can not deeply over the table in the optical axes. Therefore, the elevation angle is set to $\alpha = 75$ [deg].

Figure 13 shows the comparison of 3 types of texture patterns: the first consists of the big circles with the low density distribution; the second consists of the small circles with the high density distribution; the third consists of the middle circles with the high density distribution. The performance function of the correlation of (15) with respect the (k_i, l_i) are illustrated under the figures of the texture patterns. It is confirmed that there is only one minimum extremum in the case of the first texture while there are some minimum extrema in the other cases. Therefore, the first texture pattern is used in the next experiments.
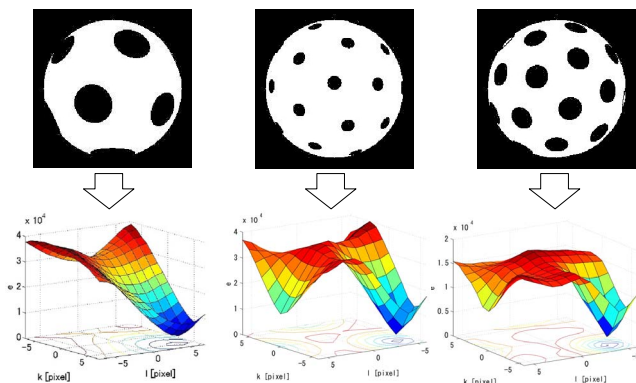

Fig. 13. The comparison of 3 types of the texture patterns.

6. EXPERIMENTS

The effectiveness of the proposed method is verified by experiments. The operating system of the computer is Windows XP sp2. The CPU is the Intel(R) Xeon(R) E5430, 2.66GHz. The physical memory is 2.00GB RAM. The autmatical ball catapult is set to the configurations of the cases of the top and back spins. The lines, markers and axes of figures in latter are same as those in the simulation results. The image data is also saved in HDD during the real-time measurement of the ball velocity. Then, the true values in the latter are manually estimated by the tracking-based method of Section 3 in off-line. Figure 14 shows an example of some parts $(n = 1, \cdots, 6)$ of the saved image data of the expperiment of the real-time
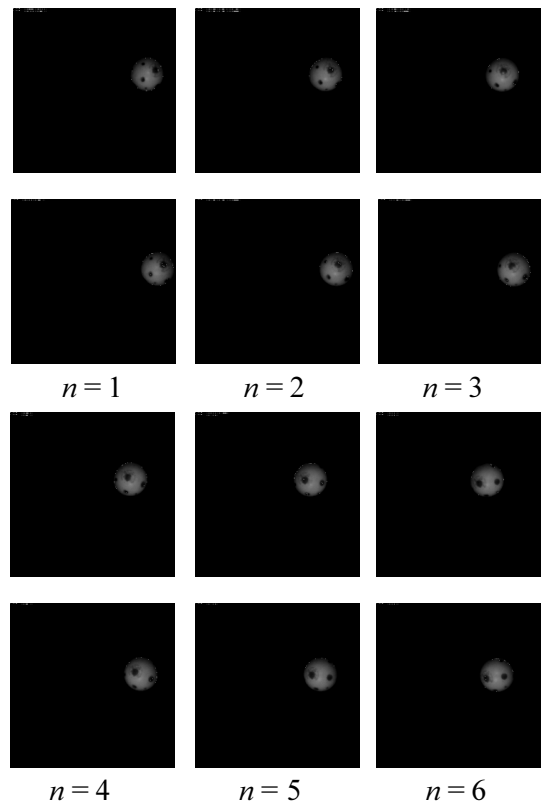

Fig. 14. An example of the experimental image data.

measurement. The upper and lower figures represent the left and right image data respectively. The translational and rotational velocities of the ball are estimated by the real-time measurement in on-line.

Fig.15 shows the experimental result of the translational velocity of the ball in the x-axis. It is confirmed that the measured values coincide with the true values well. Figs. 16, 17 show the results the axis and speed of the rotational velocity. In Fig. 16, the angles between almost the measured axes and the true axis are smaller than 45 [deg]. In Fig. 17, there is the significant deviation of about 700 [rpm] between the measured and true values of the rotational speed. The processing time averaged with 10 frame is 15–30 [ms], which is very shorter than the rally time of 200–500 [ms]. Therefore, the remaining time is long enough to predict the ball trajectory and plane the racket trajectory.

7. CONCLUSIONS

We proposed the real-time measuring method of both the translational/rotational velocities of a flying ball using the two high speed cameras. The rotational velocity was estimated by the kinematics which relates the velocity to the position variation of the centroid of a feature area marked on the ball. The position variation was calculated by the correlation between two images with respect to the translational displacement in the images. The corresponding 3D position of the feature area was calculated by the centroids of all the feature areas on the ball in the left and right images with the assumption where the centroids coincide with each other in the 3D space. The proposed method was verified with respect to the configurations
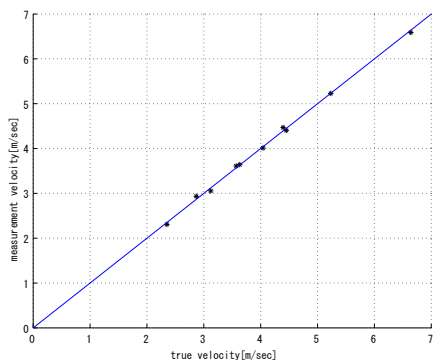
Fig. 15. The experimental result of the translational velocity in the x-axis.
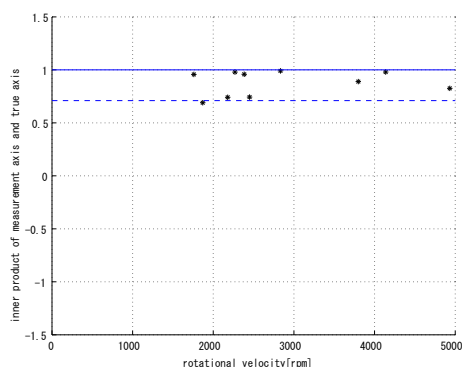
Fig. 16. The experimental result of the rotational axis.
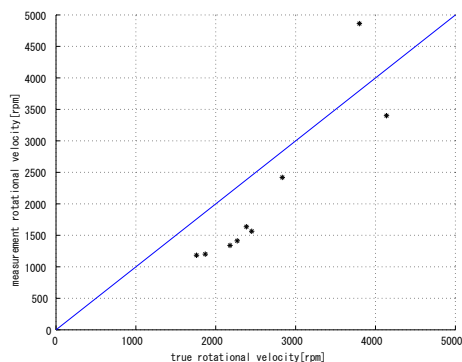
Fig. 17. The experimental result of the rotational speed.

of the cameras and the texture patterns of the feature areas by the numerical simulations. The effectiveness of the method was verified by the experiments.

The processing time is short enough for a robot to play table tennis. However, it is necessary to improve the accuracy of the measured rotational velocity because it is not high enough. An idea is to consider both the kinematic relation and the image registration in the estimation.

REFERENCES

Ishii, I., Nakabo, Y., and Ishikawa, M. (1996). Target tracking algorithm for 1ms visual feedback system using massively parallel processing. In *Proc. IEEE Int. Conf. Robot. Automat.*, 2309–2314.

Murray, R.M., Li, Z., and Sastry, S.S. (1994). *A Mathematical Introduction to ROBOTIC MANIPULATION*. CRC Press.

Nakabo, Y., Ishii, I., and Ishikawa, M. (1996). High speed target tracking using 1ms visual feedback system. In *Video Proc. IEEE Int. Conf. Robot. Automat.*, 6.

Nakashima, A., Kobayashi, Y., Ogawa, Y., and Hayakawa, Y. (2009). Modeling of rebound phenomenon between ball and racket rubber with spinning effect. In *Proc. ICCAS-SICE 2009*, 2295–2300.

Nakashima, A., Ogawa, Y., Kobayashi, Y., and Hayakawa, Y. (2010). Modeling of rebound phenomenon of a rigid ball with friction and elastic effects. In *Proc. IEEE Amer. Cont. Conf.* (To be published).

Szeliski, R. (1994). Image mosaicing for tele-reality applications. Tech. rep. crl 94/2, Digital Equipment Corporation, Cambridge Research Lab.

Tamaki, T., Sugino, T., and Yamamoto, M. (2004). Measuring ball spin by image registration. In *Proc. 10th Frontiers of Computer Vision*, 269–274.

Watanabe, Y., Komuro, T., Kagami, S., and Ishikawa, M. (2005). Multi-target tracking using a vision chip and its applications to real-time visual measurement. *Journal of Robotics and Mechatronics*, 17(2), 121–129.